# Decadal Shift in El Niño Influences on Indo–Western Pacific and East Asian Climate in the 1970s*

SHANG-PING XIE,[+] YAN DU,[#] GANG HUANG,[@] XIAO-TONG ZHENG,[&] HIROKI TOKINAGA,[+] KAIMING HU,[@] AND QINYU LIU[&]

[+] *International Pacific Research Center, and Department of Meteorology, University of Hawaii at Manoa, Honolulu, Hawaii*
[#] *LED, South China Sea Institute of Oceanology, Chinese Academy of Sciences, Guangzhou, China*
[@] *LASG, Institute of Atmospheric Physics, Chinese Academy of Sciences, Beijing, China*
[&] *Ocean University of China, Qingdao, China*

(Manuscript received 14 September 2009, in final form 28 December 2009)

ABSTRACT

El Niño's influence on the subtropical northwest (NW) Pacific climate increased after the climate regime shift of the 1970s. This is manifested in well-organized atmospheric anomalies of suppressed convection and a surface anticyclone during the summer (June–August) of the El Niño decay year [JJA(1)], a season when equatorial Pacific sea surface temperature (SST) anomalies have dissipated. In situ observations and ocean–atmospheric reanalyses are used to investigate mechanisms for the interdecadal change. During JJA(1), the influence of the El Niño–Southern Oscillation (ENSO) on the NW Pacific is indirect, being mediated by SST conditions over the tropical Indian Ocean (TIO). The results here show that interdecadal change in this influence is due to changes in the TIO response to ENSO.

During the postregime shift epoch, the El Niño teleconnection excites downwelling Rossby waves in the south TIO by anticyclonic wind curls. These Rossby waves propagate slowly westward, causing persistent SST warming over the thermocline ridge in the southwest TIO. The ocean warming induces an antisymmetric wind pattern across the equator, and the anomalous northeasterlies cause the north Indian Ocean to warm through JJA(1) by reducing the southwesterly monsoon winds. The TIO warming excites a warm Kelvin wave in tropospheric temperature, resulting in robust atmospheric anomalies over the NW Pacific that include the surface anticyclone. During the preregime shift epoch, ENSO is significantly weaker in variance and decays earlier than during the recent epoch. Compared to the epoch after the mid-1970s, SST and wind anomalies over the TIO are similar during the developing and mature phases of ENSO but are very weak during the decay phase. Specifically, the southern TIO Rossby waves are weaker, so are the antisymmetric wind pattern and the North Indian Ocean warming during JJA(1). Without the anchor in the TIO warming, atmospheric anomalies over the NW Pacific fail to develop during JJA(1) prior to the mid-1970s. The relationship of the interdecadal change to global warming and implications for the East Asian summer monsoon are discussed.

## 1. Introduction

Summer (June–August) is the major rainy season for the subtropical northwest (NW) Pacific and East Asia. Rainfall variability during summer is of great socioeconomic importance for East Asia. Summer rainfall in the region displays peculiar correlations with the El Niño–Southern Oscillation (ENSO), not concurrently but eight months after sea surface temperature (SST) anomalies in the equatorial Pacific have peaked (Huang and Wu 1989; Zhang et al. 1996; Wang et al. 2003; Huang et al. 2004; Arai and Kimoto 2008). In the summer following an El Niño event, precipitation decreases over the subtropical NW Pacific and tends to increase over eastern China and Japan. The meridional dipole of rainfall anomalies in the East Asia–western Pacific sector is a signature of the so-called Pacific–Japan (PJ) pattern, best seen in low-level vorticity and upper-level height fields (Nitta 1987; Kosaka and Nakamura 2006). The correlation between the PJ pattern and ENSO must be anchored by SST forcing, but the search for SST forcing within the tropical Pacific turns out not very successful (Nitta 1990; Kosaka and

* International Pacific Research Center Publication Number 669 and School of Ocean and Earth Science and Technology Publication Number 7889.

*Corresponding author address:* Shang-Ping Xie, IPRC, SOEST, University of Hawaii at Manoa, Honolulu, HI 96822.
E-mail: xie@hawaii.edu

DOI: 10.1175/2010JCLI3429.1

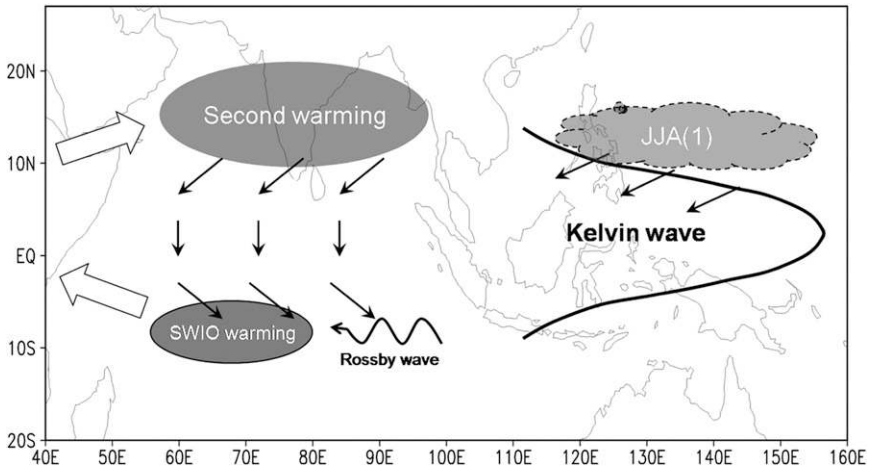


FIG. 1. Schematic of El Niño teleconnection into the Indo–NW Pacific: as downwelling Rossby waves propagate into the southwest TIO thermocline ridge, the SST warming there induces an antisymmetric wind pattern (arrows), which weakens the prevailing southwesterlies (block arrow on the left) and causes the NIO to warm in summer. The TIO warming excites a warm Kelvin wave in tropospheric temperature, inducing surface wind divergence and suppressing convection in the subtropical NW Pacific during JJA(1).

Nakamura 2006; Xie et al. 2009). El Niño typically dissipates by the summer, a time when SST anomalies over the NW Pacific tend to be negatively correlated with local rainfall during summer (Wang et al. 2005).

Recent studies point to tropical Indian Ocean (TIO) SST anomalies as the anchor of the PJ pattern via the following capacitor effect (Yang et al. 2007; Xie et al. 2009). TIO SST increases in response to the atmospheric teleconnection by El Niño [Klein et al. 1999; Alexander et al. 2002; see Schott et al. (2009) for a recent review], like a battery charging a capacitor. The TIO warming persists and exerts influences on NW Pacific climate like a discharging capacitor, especially during summer when El Niño has dissipated. The schematic in Fig. 1 illustrates the capacitor effect. Specifically, the TIO warming forces a Matsuno–Gill pattern in tropospheric temperature. A warm Kelvin wave propagates into the equatorial western Pacific, inducing northeasterly surface wind anomalies on the northern flank of the Kelvin wave under surface friction. The frictional-induced subtropical divergence suppresses convection, and the ensuing feedback between convection and circulation gives rise to an anomalous anticyclone in the lower troposphere. This Kelvin wave–induced Ekman divergence (WIED) mechanism favors the northern flank of the equatorial Kelvin wave because summer convection and hence convective feedback are stronger in the Northern than Southern Hemisphere (Xie et al. 2009). A similar mechanism is invoked to explain the influence of tropical Atlantic SST anomalies on Indian summer monsoon rainfall (Kucharski et al. 2009). Elements of the TIO capacitor effect and the Kelvin WIED mechanism have been hinted at in earlier studies (Wu and Liu 1995; Terao and Kubota 2005; Ohba and Ueda 2006). In a coupled ocean–atmosphere forecast model, replacing TIO SST with climatology substantially weakens the atmospheric Kelvin wave wedge from the TIO and reduces the magnitude of atmospheric anomalies over the NW Pacific by 50% during the summer (June–August) of the ENSO decay year [JJA(1)] (Chowdary et al. 2010). Our convention is that years 0 and 1 denote the developing and decay years of an ENSO event, respectively. Seasons referred to are for the Northern Hemisphere.

Local ocean–atmosphere interactions play an important role in shaping spatiotemporal structures of the TIO response to ENSO. SST warming displays a peculiar double peak structure over the north Indian Ocean (NIO) and South China Sea (SCS), one at the mature phase of El Niño and one during June–July(1) (Du et al. 2009). The second warming peak is perplexing as it occurs after El Niño has dissipated. Du et al. identify an equatorially antisymmetry pattern of wind anomalies as key to the NIO warming during summer by relaxing the prevailing southwest monsoon and reducing surface evaporation. They show that the wind pattern is in turn anchored by the persistent SST warming over the southwest TIO, where the thermocline is shallow and slow propagating ocean Rossby waves are the major mechanism for SST variability (Xie et al. 2002; Huang and Kinter 2002). These results support the wind-induced evaporation mechanism of Klein et al. (1999) for NIO SST variability but trace the origin of wind anomalies to slow ocean dynamical adjustments in the south TIO.

Indo–Pacific climate displays a marked change across the mid-1970s (Nitta and Yamada 1989; Trenberth and Hurrell 1994). This climate regime shift is best seen in the midlatitude North Pacific (Deser and Blackmon 1995; Minobe 1997; Mantua et al. 1997; Taguchi et al. 2007) but with coherent ocean–atmospheric anomalies over the tropical Indo–Pacific Oceans (Zhang et al. 1997; Garreaud and Battisti 1999; Deser et al. 2004). For convenience, the period prior to (post) the mid-1970s climate regime shift is called the PRE (POST) epoch. Systematic changes have been documented in summer monsoons from India to the NW Pacific. Over China, the POST − PRE epoch difference in summer rainfall displays a pattern of wet south and dry north across the mid-1970s, with northerly wind anomalies over eastern China [see Zhou et al. (2009) for a recent review]. The correlation of summer Chinese rainfall with ENSO experiences significant changes (Chang et al. 2000). The correlation of all Indian rainfall with ENSO during its developing phase has deteriorated (Kumar et al. 2006), possibly because of more frequent occurrence after the mid-1970s of El Niño Modoki with SST anomalies trapped in the central equatorial Pacific (Trenberth and Smith 2006; Ashok et al. 2007). ENSO influences on Australian rainfall also weaken in the POST epoch (Power et al. 1999).

The correlation of the NW Pacific summer monsoon with ENSO strengthens after the mid-1970s (Wu and Wang 2002), a change hypothesized owing to enhanced ENSO activity (Wang et al. 2008). The exact mechanisms for this interdecadal strengthening of the ENSO teleconnection to the subtropical NW Pacific remain unclear. Most studies of interdecadal changes are based on atmospheric reanalyses, which are known to suffer spurious changes across the 1970s (e.g., Wu and Xie 2003) most likely because of substantial increase and assimilation of satellite data.

The present study investigates processes that cause ENSO teleconnection to the Indo–western Pacific during summer to change across the 1970s. Our analysis of ship observations confirms that such interdecadal changes took place. Our results point to TIO processes and their influences on the NW Pacific. We show that the ENSO teleconnection at its decay phase strengthens over the TIO from the PRE to POST epoch, and the enhanced TIO warming forces more robust JJA(1) anomalies of the atmosphere over the NW Pacific. These results are consistent with and extend recent studies of the TIO capacitor effect on summer NW Pacific climate (Du et al. 2009; Xie et al. 2009). The PRE epoch illustrates that, when the TIO warming is not strong during JJA(1), NW Pacific climate anomalies such as the anticyclone fail to develop.

The rest of the paper is organized as follows: Section 2 describes the data and analysis methods. Section 3 documents changes in ENSO correlations over the Indo–western Pacific Oceans, while section 4 investigates changes in ocean–atmospheric processes for the changes over the TIO. Section 5 discusses changes in East Asian rainfall variability. Section 6 is a summary and discusses implications of this study.

## 2. Data and methods

### *a. Observations*

We use atmospheric reanalyses by the U.S. National Centers for Environmental Prediction/National Center for Atmospheric Research (NCEP–NCAR) (NRA; Kalnay et al. 1996) and by the European Centre for Medium-range Weather Forecasts (ECMWF) (ERA; Uppala et al. 2005), available on a 2.5° grid for 1948–2008 and 1958–2001, respectively. Although the same numerical models are used to interpret observations, the assimilated data are far from homogeneous, improving over time in both quality and quantity especially after the 1970s when the satellite era begins.

The international Comprehensive Ocean–Atmospheric Dataset (iCOADS) (Worley et al. 2005) is a collection of surface meteorological observations by ships. We have gridded these ship reports onto a 5° latitude by 10° longitude grid. All features to be discussed have large zonal scales, and the coarse zonal grid spacing is to help suppress small-scale variability. Grid points without at least one observation for a given month are flagged as missing. We limit our analysis to after 1950 when observations are relatively abundant. SST, surface wind velocity, and sea level pressure (SLP) from iCOADS are used as an independent check against atmospheric reanalyses for interdecadal change.

To extend the precipitation record back beyond the satellite era that began in 1979, monthly observations at Guam are used to track rainfall over the subtropical NW Pacific. We average data at five stations to form an island-mean precipitation series, which runs nearly continuously since 1945. A different method by normalizing data at each station with its standard deviation yields a similar island-mean series.

We use three global precipitation products based on rain gauge observations over land from the University of Delaware (UD) (Legates and Willmott 1990), Climate Prediction Center (CPC) (Chen et al. 2002), and Global Precipitation Climatology Centre (GPCC) (Rudolf and Schneider 2005), available since 1900 on a 0.5° grid. To suppress noise, we have regridded the data onto a 2.5° grid by simple averaging.

For interannual variability in the thermocline depth, we use the Simple Ocean Data Assimilation (SODA) product version 2.0.2, available since 1958 (Carton and Giese 2008). ERA is used as surface forcing in SODA. SODA compares very well with expendable bathythermograph (XBT) observations in the TIO (Xie et al. 2002). We supplement SODA with an optimally interpolated temperature product for upper 400 m (White 1995), available from the Scripps Institution of Oceanography on a 2° latitude × 5° longitude grid since 1954. Both the SODA and White products are affected by change in sampling associated with the widespread use of XBT and CTD since the 1970s. The White product is global but effectively limited to north of 25°S in the Indian Ocean. As an independent check, we use a free-running hindcast by the ocean GCM for the Earth Simulator (OFES) with NRA as surface forcing (Sasaki et al. 2008; Taguchi et al. 2007).

The present study focuses on interannual variability associated with ENSO. To reduce the effect of intraseasonal variability over the Indo–western Pacific oceans, we apply a three-month running average. A 9-yr running mean is then applied (separately for each calendar month) to remove decadal and longer variations, which are significant over the tropical Indo–Pacific oceans (Deser et al. 2004; Du and Xie 2008). All interannual anomalies, for both observations and model simulations, are obtained by using this 3-month to 9-year bandpass filter. We use SST averaged over the eastern equatorial Pacific (Niño-3.4: 5°S–5°N, 120°–170°W) to track ENSO, which is referred to as the ENSO index. The autocorrelation of the bandpass-filtered ENSO index falls to zero at a lag of 8 months, leading us to estimate the effective degree of freedom as (analysis period in years) per 1.5 years. For a 21-year time series, a correlation of 0.53 reaches the 95% significance level based on a $t$ test (equivalent to 5% confidence level to reject the null hypothesis of no correlation).

### *b. Atmospheric simulations*

A 21-member ensemble simulation is conducted for 1950–2000 with the NCAR Community Atmosphere Model version 3 (CAM3). Each member is forced by the same, observed history of SST based on the Met Office Hadley Centre Sea Ice and SST Dataset (HadISST) and differs in atmospheric initial conditions. CAM3 uses an Eulerian spectral dynamical core and includes physical packages for convection, turbulence, and cloud (Collins et al. 2004). The model uses triangular truncation at T42 (equivalent grid spacing of 2.8°) and has 26 vertical levels.

A pair of auxiliary simulations is performed with the ECHAM5, one forced with observed SST for 1958–2000 over the global domain (ECHAM-GOGA) and one with interannual SST anomalies only over the Indian Ocean (ECHAM-IOGA). Only one integration each is available. ECHAM5 is the new Hamburg version of the ECMWF model. A detailed description of ECHAM5 is given by Roeckner et al. (2003). ECHAM5 employs a spectral dynamic core. We use a version with triangular truncation at zonal wavenumber 63 (T63, equivalent to 1.9° horizontal resolution) and 19 sigma levels in the vertical.

## 3. Northwest Pacific climate anomalies

Figure 2a shows the 21-year running correlation of NW Pacific SLP with the November(0)–January(1) [NDJ(0)] Niño-3.4 SST index based on iCOADS ship observations, for the ENSO decay year [year(1)] as a function of year and calendar month. (The years in Fig. 2 denote the centers of sliding windows; e.g., 1960 represents the correlation in the 21-year sliding window of 1950–70.) Positive SLP anomalies develop over the NW Pacific at the mature phase of El Niño (Harrison and Larkin 1996; Wang et al. 1999), accompanied by an anomalous anticyclonic circulation near the surface. The subsequent evolution of this anomalous high displays a pronounced interdecadal change around the mid-1970s. While the anticyclonic anomalies are observed over the subtropical NW Pacific during JJA(1) (Wang et al. 2003) especially for the CPC Merged Analysis of Precipitation (CMAP) era since 1979 (Xie et al. 2003), JJA(1) SLP correlation with ENSO falls below the 95% significance level ($r = 0.53$) prior to the mid-1970s. Roughly, significant SLP correlation ($r > 0.53$) lasts two to three months longer after than before the mid-1970s. This result confirms the interdecadal change in JJA(1) NW Pacific response to ENSO detected by Wang et al. (2008) from atmospheric reanalyses. Such confirmation is significant as our analysis is based on ship observations free of possible spurious shifts due to changes in data–model assimilation.

Rainfall at Guam (13.5°N, 145°E) is used as an independent check for interdecadal change in ENSO influences. August–October is the major rainy season for Guam, with monthly rainfall exceeding 300 mm as opposed to ~100 mm in January–April. The 21-year running correlation between JJA(1) Guam rainfall and the NDJ(0) ENSO index strengthens in the 1960s to highly significant values of 0.6–0.7 after the mid-1970s (Fig. 2b). The standard deviation of JJA rainfall is quite large at 93 mm month$^{-1}$ for the recent 30 years, one-third of the climatological mean (288 mm month$^{-1}$). The correlation displays several other changes across the mid-1970s; the maximum shifts from JFM(1) to JJA(1), and significant correlation begins to emerge for JAS(1) after

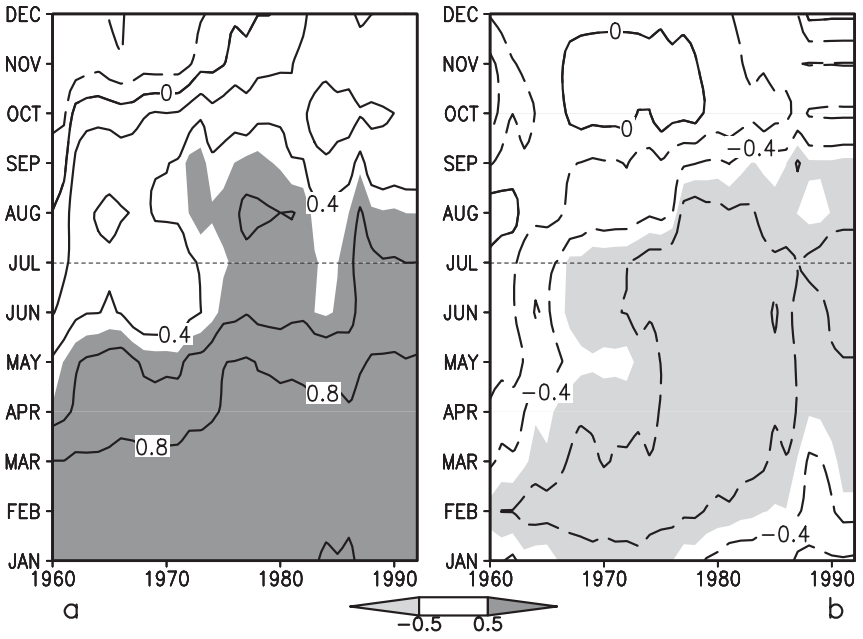


FIG. 2. Twenty-one-year running correlation with the NDJ(0) Niño-3.4 SST index as a function of year and calendar month for the decay year of ENSO: (a) SLP over the subtropical NW Pacific (10°–25°N, 130°–170°E) and (b) rainfall at Guam. Values exceeding the 95% significance level are shaded.

the 1976. Guam observations corroborate that ENSO exerts a stronger control on NW Pacific climate after the mid-1970s during the summer following an ENSO event.

Clouds in the Indo–western Pacific warm pool are dominated by those associated with deep convection. Without satellite estimates over the ocean prior to 1979, we use ship observations of cloudiness in iCOADS as a proxy for precipitation to cover a 57-year period of 1950–2006 (Deser et al. 2004). Figures 3a,b show the first and second empirical orthogonal function (EOF) modes of JJA cloudiness variability over the eastern Indian and western Pacific oceans, which explain 15% and 8% of total variance, respectively. The spatial patterns are nearly identical to precipitation patterns for JJA(0) and JJA(1) based on post-1979 satellite estimates (e.g., Fig. A1 of Xie et al. 2009). Cloud EOF 1 represents an east–west dipole between the Pacific and Maritime Continent, characteristic of the eastward shift of the atmospheric convection center at the developing phase of El Niño. EOF 2 features a reduction in cloud in the subtropical NW Pacific and an increase around Japan, reminiscent of the PJ pattern. The correlation of the first principal component (PC) with the NDJ(0) ENSO index is high throughout the analysis period in a narrow range of 0.6–0.7 (Fig. 3c). Cloud PC-2 correlates with the ENSO index seven months ago [NDJ(0)], and the correlation displays a rapid rise in the 1970s from 0.4 to around 0.6. [The dip in correlation in the 1980s may have to do with a decrease in ENSO variability (section 3b).] The nearly constant and high correlation of cloud PC-1 and ENSO indicates it unlikely that the rise of PC-2 correlation is due to sampling variations in iCOADS. Rather, the cloudiness analysis supports the results at Guam that ENSO influences on NW Pacific rainfall have strengthened since the 1970s during the summer following ENSO decay.

### *a. TIO warming and atmospheric Kelvin wave*

Upper panels of Fig. 4 compare JJA(1) SST, SLP, and surface winds in plan view over the Indo–Pacific oceans for the POST and PRE epochs, based on iCOADS. During the recent epoch, the TIO warming is highly significant and its correlation with NDJ(0) El Niño events exceeds 0.6 over much of the basin. SLP decreases over the TIO (although marginal in statistical significance), and a low SLP wedge extends eastward toward the western Pacific on the equator, suggesting an atmospheric Kelvin wave. Over the NW Pacific, there is a pronounced anticyclonic circulation in the subtropics and a cyclonic circulation over Japan, reminiscent of the meridional PJ pattern. SLP rises over the subtropical NW Pacific, consistent with the circulation anomalies. [Regression patterns for SLP and circulation are nearly in geostrophic balance (not shown).] Prior to the mid-1970s, by contrast, the TIO warming is significantly weaker, by 0.2

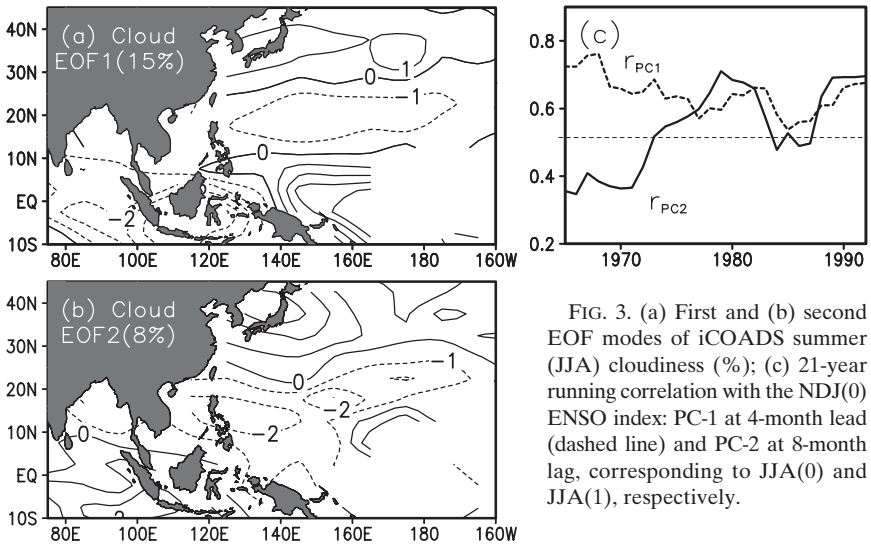


FIG. 3. (a) First and (b) second EOF modes of iCOADS summer (JJA) cloudiness (%); (c) 21-year running correlation with the NDJ(0) ENSO index: PC-1 at 4-month lead (dashed line) and PC-2 at 8-month lag, corresponding to JJA(0) and JJA(1), respectively.

in correlation. In the NW Pacific, circulation anomalies are not well defined in iCOADS, and SLP correlation drops to below 0.4. Overall, SST, SLP, and wind anomalies are similar in spatial pattern between the epochs but strengthen in ENSO correlation since the mid-1970s.

Lower panels of Fig. 4 compare tropospheric temperature anomalies averaged between 850 and 250 hPa during JJA(1), based on ERA. For the POST epoch, the tropospheric warming displays a Matsuno (1966)–Gill (1980) pattern in the Indo–western Pacific sector, with a broad meridional structure over the TIO with off-equatorial maxima suggestive of baroclinic Rossby waves. The warming wedges into the western Pacific with an equatorial maximum characteristic of the Kelvin wave. A surface anticyclone and suppressed convection are found north of the Kelvin wave wedge, consistent with the Kelvin WIED mechanism of Xie et al. (2009). For the PRE epoch, tropospheric warming is weaker by 0.2 in correlation. The pattern, still reminiscent of the Matsuno–Gill solution, is zonally confined and shifted eastward compared to the POST epoch. The pattern shift seems consistent with the SST cooling in the western equatorial Indian Ocean (Fig. 4b) and is suggestive of a heating source centered over the Maritime Continent. Over the NW Pacific, convective anomalies are not significant, consistent with changes in rainfall correlation at Guam. Along 10°N, northeasterly wind anomalies are much stronger in ERA than in iCOADS, suggesting that the assimilation model produces too strong a response to TIO warming when weakly constrained by few observations in the PRE epoch.

We have also examined NRA. The tropospheric warming is similar for the POST epoch between the two reanalyses (e.g., Fig. 9 of Xie et al. 2009) but much stronger in NRA than in ERA for the PRE epoch. The reduction in overall correlation from the POST to PRE epoch is about 0.2 in ERA but less than 0.1 in NRA. We then turn to long-term atmospheric soundings at Singapore, available since 1955. Singapore is conveniently located near the equatorial center of the Matsuno–Gill pattern of JJA(1) tropospheric warming. The correlation of summer tropospheric temperature at Singapore with the NDJ(0) ENSO index increases steadily from the late 1960s to 1980s, from 0.4 to 0.8 (Fig. 5). This interdecadal change in Singapore correlation is more consistent with ERA than NRA. The inconsistency between NRA and ERA and with Singapore soundings illustrates that caution is needed to study interdecadal variations using reanalyses.

The Singapore sounding results lead us to conclude that JJA(1) tropospheric warming becomes more robust for the POST than PRE epoch, much as the SST warming over the TIO does. This conclusion is consistent with a longer persistence of El Niño–induced tropospheric warming for the POST than PRE epoch in an earlier analysis of atmospheric sounding data by Kubota and Terao (2004). Most of their sounding stations are in the Indo–western Pacific sector.

Over the TIO, the JJA(1) rainfall response is not well organized in space (Fig. 4c) but the correlation with the NDJ(0) ENSO index increases to 0.6 if the basin mean is used, a value above the 95% significance for a 28-year period 1979–2007. While tropospheric temperature anomalies resemble the Matsuno–Gill pattern, the surface circulation response is more complicated than depicted by the simple model of a single baroclinic mode with the resting mean state. The circulation anomalies nevertheless are largely reproducible in a dry model that considers more vertical modes and sheared mean

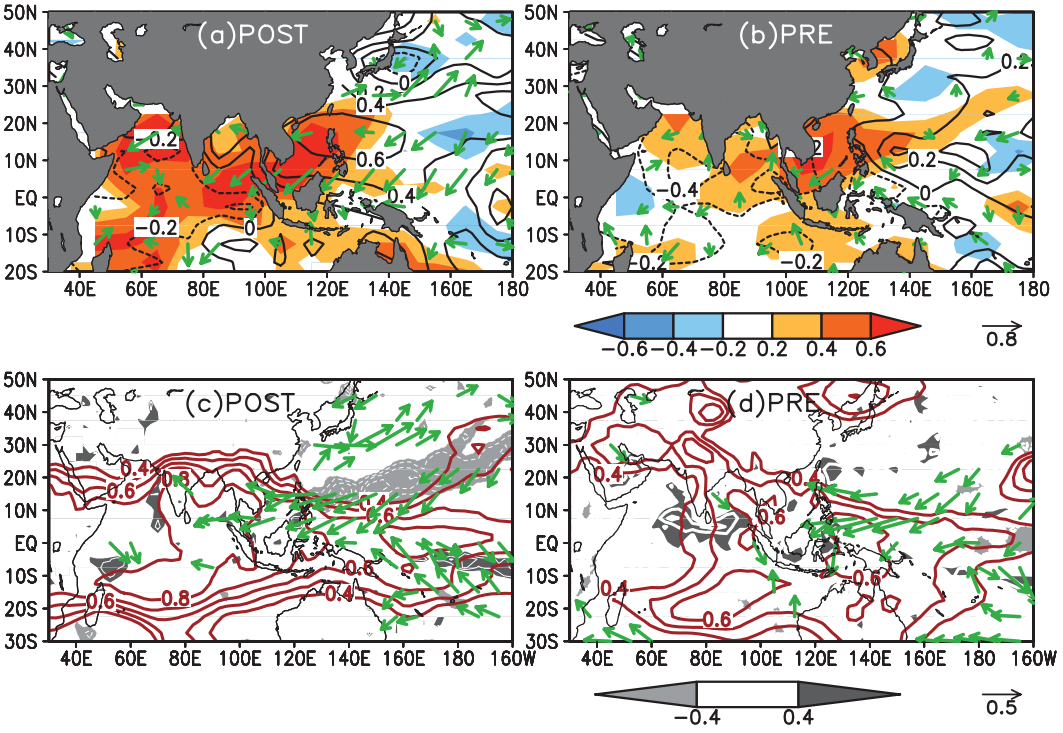


FIG. 4. Correlation of JJA(1) SST (color), SLP (contours), and surface wind velocity (vectors) with the NDJ(0) Niño-3.4 SST index for the (a) POST (1977–2003) and (b) PRE (1950–76) epochs. The JJA(1) tropospheric temperature (red contours), and convective rainfall (gray shade > 0.4 and white contours at intervals of 0.1), for the (c) POST (1980–2001) and (d) PRE (1958–79) epochs. (top), (bottom) Green vectors show the correlation (regression) of surface wind velocity based on iCOADS (ERA).

flow if both latent heating over the TIO and cooling over the NW Pacific are prescribed (Fig. 11b of Xie et al. 2009). In the moist atmosphere, the TIO heating causes the NW Pacific cooling via Kelvin WIED. Further studies are necessary to clarify the effects of mean flow and modes other than the first baroclinic mode.

### b. *Model simulations*

The interdecadal changes in ENSO influences may be due to SST changes and/or atmospheric chaotic variability. Atmospheric GCM hindcasts can clarify the relative importance of these possibilities. SST-forced hindcasts with both CAM3 and ECHAM5 corroborates the role of TIO SST. Figure 6 shows JJA correlation in probability density function (pdf) between TIO SST and a NW Pacific anticyclone index for 21 CAM3 hindcasts during PRE and POST epochs. Without exception, the correlation is higher for the POST than PRE epoch in all of the 21 simulations. The correlation coefficient for the ensemble mean is −0.2 for 1957–76, and 0.6 for 1977–96.

The ECHAM5 simulations, albeit with only one member, are consistent with the CAM3 result. In the GOGA run forced by global SST variations, the correlation between TIO SST and NW Pacific anticyclone rises from 0.37 for the PRE to 0.49 for the POST epoch (Table 1). The latter value is just shy from the 95% significance level for a 19-year-long record. In the IOGA run prescribing interannual SST variability only over the TIO, the correlation remains largely unchanged at 0.47 for the POST but drops to nearly zero for the PRE epoch. The results from CAM3 and ECHAM5 indicate that SST changes, specifically those over the TIO, are the culprit for the strengthened ENSO influences on NW Pacific climate during JJA(1) from the PRE to POST epoch.

### c. *Interdecadal changes*

We now return to observations and examine interdecadal variations in ENSO teleconnection. Figure 7a shows 21-year running correlations of TIO SST and subtropical NW Pacific SLP for JJA(1) with the NDJ(0) ENSO index. TIO SST correlation is insignificant prior to 1975, exceeds the 95% significance level ($r = 0.5$) in the second half of the 1970s, and continues to rise through the 1980s to 0.8. ENSO correlation of JJA(1) NW Pacific SLP follows a similar rising trend from the 1960s. During JJA(1) when Pacific SST anomalies are weak (Xie et al. 2009), the simultaneous rise of TIO SST and NW Pacific SLP correlations since the 1970s suggests

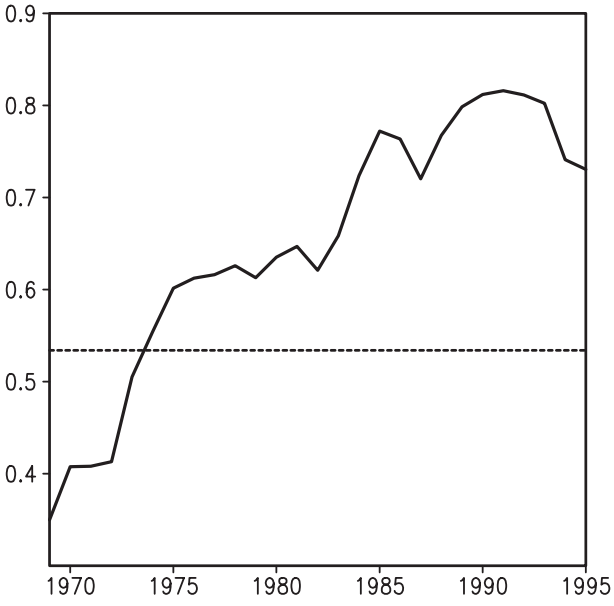


FIG. 5. Twenty-one-year running correlation with ENSO of JJA(1) tropospheric temperature at Singapore: dashed line denotes the 95% significant level.

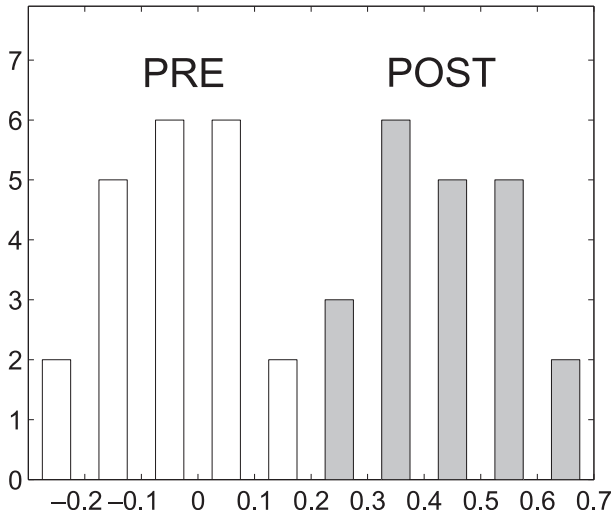


FIG. 6. Histogram of JJA correlation between TIO SST and NW Pacific anticyclone in 21-member CAM3 hindcasts for the PRE (1957–76: open bars) and POST (1977–96: gray shaded) epochs. The NW Pacific anticyclone index is defined as the difference in 850-hPa zonal wind between the regions 20°–30°N, 110°–140°E and 5°–15°N, 100°–130°E.

that the strengthening of TIO response to ENSO intensifies NW Pacific atmospheric anomalies during JJA(1).

What causes the ENSO teleconnection to the Indo–NW Pacific to strengthen? First, ENSO activity has intensified from the 1960s through the 1970s, with the standard deviation of NDJ(0) Niño-3.4 SST from 1.0° to nearly 1.3°C (Fig. 7b). Second, El Niño lasts longer; correlation between MAM(1) and NDJ(0) Niño-3.4 SST rises from below 0.6 to above 0.8 from the 1960s to 1990s (Fig. 7a). These ENSO changes are accompanied by a rise in JJA variance of TIO SST and NW Pacific SLP, suggesting the former causing the latter. The slow decay of ENSO during the POST epoch, especially, is an overlooked aspect of interdecadal ENSO change [see An (2009) for a recent review] but, as we will show, helps strengthen ENSO teleconnection into the TIO.

## 4. Indian Ocean response

Diagnostic and GCM results in section 3 show that the TIO response to ENSO and its influence on the NW Pacific summer climate strengthened across the mid-1970s. This section investigates ocean–atmospheric processes leading to the changes in TIO response to ENSO.

The persistence of El Niño-induced TIO warming has changed substantially. Figure 8 compares lagged correlation with ENSO of SST averaged over the TIO and its subbasins between the PRE and POST epochs. For the POST epoch, the basin warming persists through JJA(1), and NIO SST anomalies feature a pronounced peak in June(1). For the PRE epoch, by contrast, the second summer warming of the NIO is missing. Diagnostic and modeling results of Xie et al. (2009) show that positive NIO SST anomalies are the major anchor for the JJA(1) anomalous anticyclone over the subtropical NW Pacific, suggesting that the lack of the second summer peak of the NIO warming may hold the key to the weakened TIO influences for the PRE epoch.

TIO–atmosphere interaction is important for the second peak of the NIO warming during JJA(1) (Izumo et al. 2008; Du et al. 2009), a season when El Niño has dissipated (Fig. 8). As Fig. 1 illustrates, it involves the following sequence of adjustments. Anticyclonic wind curls associated with the El Niño teleconnection excite downwelling Rossby waves in the south TIO. As these Rossby waves propagate into the thermocline ridge over the southwest TIO, they induce positive SST anomalies

TABLE 1. JJA correlations between TIO SST and a NW Pacific anticyclone index for the PRE (1957–76) and POST (1977–96) epochs in CAM3 GOGA (21-member ensemble mean), ECHAM5 GOGA, and IOGA simulations. A three-month to nine-year bandpass filter is applied.

| Simulation | PRE | POST |
|---|---|---|
| CAM3 GOGA | −0.2 | 0.6 |
| ECHAM GOGA | 0.37 | 0.49 |
| ECHAM IOGA | −0.05 | 0.47 |

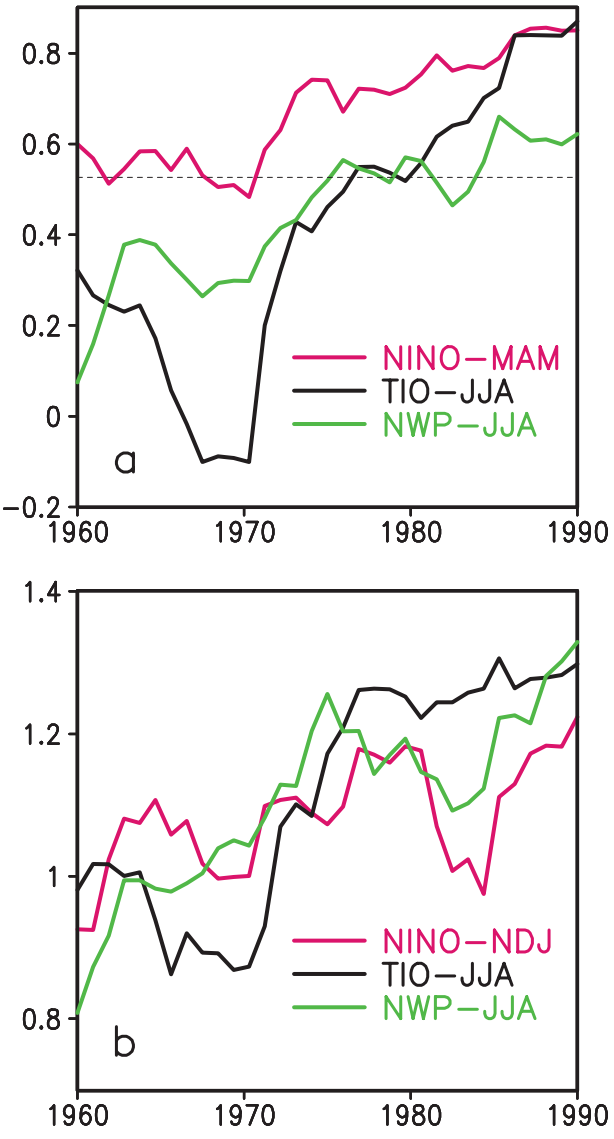


FIG. 7. (a) Twenty-one-year running correlation with the NDJ(0) ENSO index: MAM(1) Niño-3.4 SST, TIO SST and NW Pacific SLP for JJA(1); (b) 21-year running rms variance of NDJ(0) Niño-3.4 SST, TIO SST and NW Pacific SLP for JJA, normalized by their standard deviations ($\sigma$ = 1.09°C, 0.2°C, and 0.73 hPa, respectively).

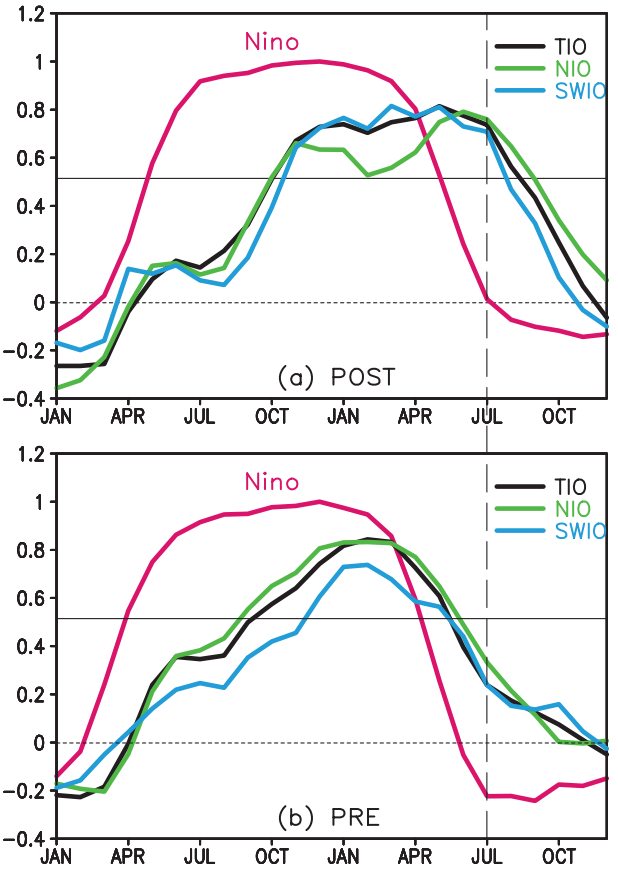


FIG. 8. Correlation with the NDJ(0) Niño-3.4 SST index during the ENSO decay year of SST over the TIO and its subbasins for (a) the POST (1977–2003) and (b) PRE (1950–76) epochs. The red line is for the lagged autocorrelation of the Niño-3.4 SST index with its NDJ(0) values.

via thermocline feedback. The SST warming over the southwest TIO propagates slowly westward and persists through the spring and early summer, driving an antisymmetric wind pattern with northeasterly anomalies over the NIO. The northeasterly wind anomalies weaken the NIO warming during winter and spring when the prevailing winds are northeasterly but then act to strengthen positive anomalies of NIO SST after the onset of the southwest monsoon. The rest of this section examines each of these processes and explores their changes across the climate regime shift.

### *a. Ocean Rossby waves*

Figure 9 shows longitude–time sections of sea surface height (SSH), SST, and Ekman pumping velocity anomalies in the south TIO, as represented by their correlation with the NDJ(0) El Niño index. SSH is based on the SODA reanalysis while SST and Ekman pumping on iCOADS. For the POST epoch, thermocline depressions begin to develop and amplify in the eastern half of the basin during September(0) to December(0) in response to in situ downwelling Ekman pumping. The Ekman pumping is associated with an anomalous anticyclone that develops over the southeast TIO during the developing phase of El Niño and/or the Indian Ocean dipole (IOD) (Xie et al. 2002; Yu et al. 2005; Rao and Behera 2005). [The IOD is the zonal mode of the equatorial Indian Ocean involving Bjerknes feedback (Saji et al. 1999; Webster et al. 1999).] The thermocline depression propagates westward slowly as Ekman downwelling persists through March(1). SST shows a strong

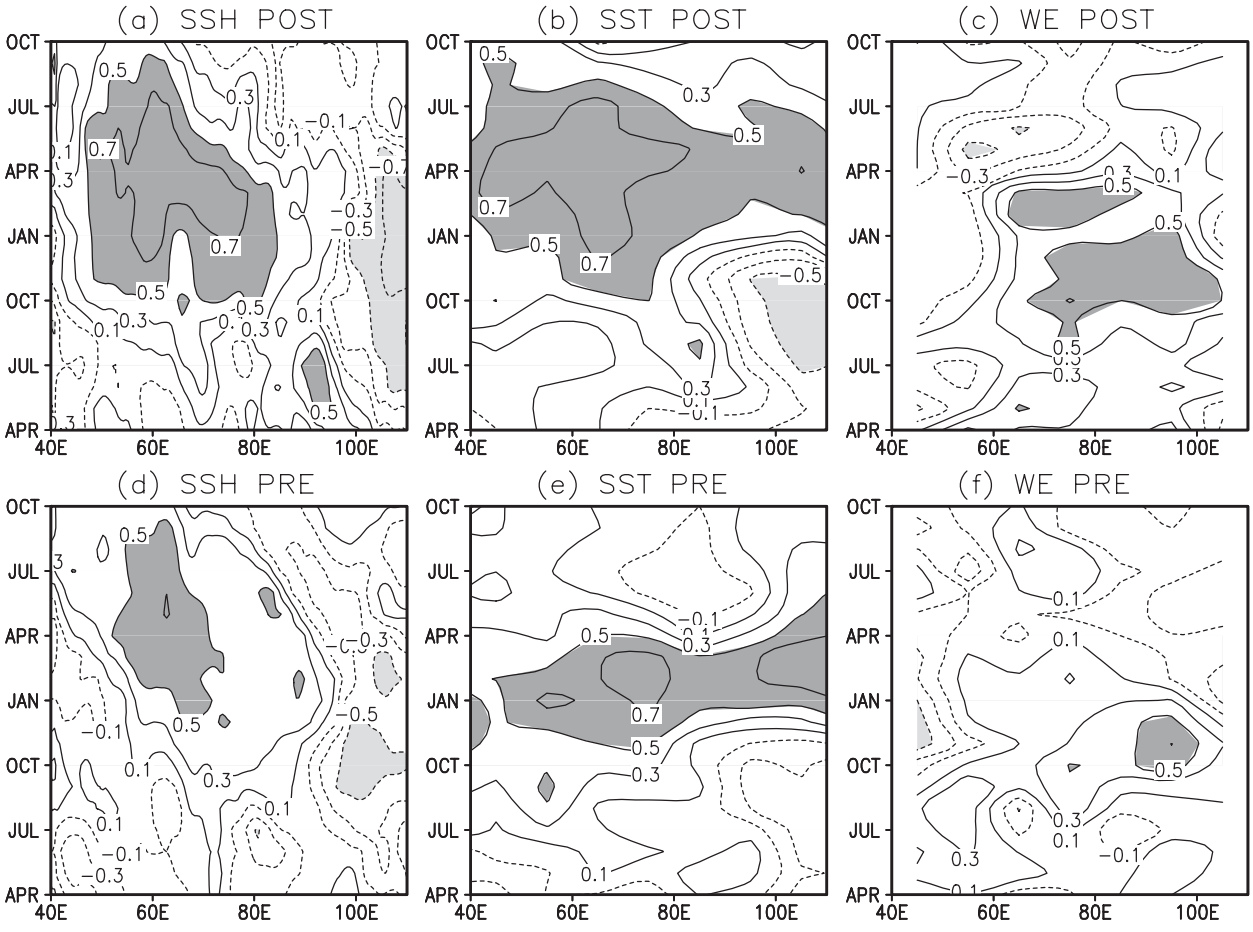


FIG. 9. Correlation with NDJ(0) Niño-3.4 SST for (upper) the POST (1980–2001) and (lower) PRE (1958–79) epochs: (left) SODA SSH, (middle) SST, and (right) Ekman pumping velocity, averaged from 5° to 15°S. SST and Ekman pumping are both based on iCOADS.

warming across the basin during February(1) to May(1). The SST warming also displays a tendency of westward copropagation with SSH anomalies, especially in the western basin where the mean thermocline is shallow and thermocline feedback is strong. The SST warming in the southwest TIO begins to decay in June(1) but remains significant until August(1). The forcing of ocean Rossby waves and their effects on SST and the local atmosphere are documented in Xie et al. (2002) and Huang and Kinter (2002).

For the PRE epoch (lower panels of Fig. 9), in comparison, the westward propagation of Rossby waves is quite clear in SSH but correlation is much weaker than for the POST epoch (left), consistent with weaker correlation in Ekman pumping (right). The basinwide warming remains significant (albeit much weaker) during January(1) to April(1) but the SST warming over the southwest TIO falls below the 95% significance level ($r = 0.53$) after April(1). The $r = 0.5$ value persists to August(1) for the POST but only to April(1) for the PRE epoch.

The enhanced persistence of southwest TIO warming for the POST epoch may be due to 1) strengthened ocean Rossby waves and/or 2) intensified thermocline feedback. The enhanced Rossby waves are consistent with strong Ekman pumping, which is in turn consistent with the increased variance and prolonged persistence of the Niño-3.4 SST index. In Fig. 8, the decay of the Niño-3.4 lagged correlation is about one month later in the POST than PRE epoch, say measured by the zero crossing. A slow-decaying El Niño in the Pacific induces easterly wind anomalies in the equatorial Indian Ocean (see the appendix), helping maintain the downwelling Ekman pumping and ocean Rossby waves. Indeed, the downwelling Ekman pumping in the central basin during January–March(1) is significant for the POST but not for the PRE epoch.

There is evidence for strengthened thermocline feedback in the southwest TIO for the POST epoch. Figure 10 shows the time series of the thermocline depth in the southwest TIO based on SODA, in good agreement with satellite SSH observations. The thermocline shoals

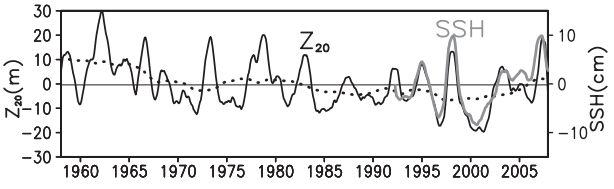


FIG. 10. Interannual anomalies of 20°C isotherm depth (black line, m) from SODA and SSH from satellite altimeters (gray line, cm) averaged in SWIO (15°–5°S, 50°–70°E). The nine-year running mean is shown with the dotted line.

by about 15 m throughout the 1970s. Similar shoaling is found in the unassimilated OFES hindcast and the upper-ocean temperature dataset of White (1995; not shown). A shoaling thermocline intensifies thermocline feedback. In addition, TIO SST displays a steady warming since the 1950s at a rate of 0.1°C decade$^{-1}$ (Alory et al. 2007; Du and Xie 2008). This secular warming is surface-intensified, helping strengthen thermal stratification and thermocline feedback. An intensified thermocline feedback is consistent with the longer persistence of SST warming over the southwest TIO thermocline ridge for the POST epoch (Fig. 9).

### b. *Antisymmetric wind pattern*

March–May is the season when El Niño is in rapid decay [MAM(1)] while TIO SST anomalies begin to exert their influence on the atmosphere. Figure 11 compares MAM(1) anomalies of SST and surface winds between the PRE and POST epochs. Over the equatorial Pacific, SST warming, and westerly wind anomalies are much stronger in the POST epoch, consistent with a slower decay of El Niño (Figs. 7 and 9). A large-scale anticyclonic circulation covers the entire subtropical NW Pacific during both epochs. SST cools significantly under the anomalous anticyclone for the POST but not the PRE epoch. The SST cooling over the subtropical NW Pacific contributes to the formation of the anomalous anticyclone (Wang et al. 2003; Lau and Nath 2003).

Over the TIO, SST warms for both epochs, but the patterns of SST and wind anomalies are very different. The POST epoch is characterized by an antisymmetric wind pattern with northeasterlies north, northwesterlies south, and northerlies on the equator. The anomalous northeasterlies cause NIO SST anomalies to decay during winter and early spring by strengthening the mean northeast monsoon while the northwesterlies help strengthen SST warming in the southwest TIO by reducing the southeast trades (Kawamura et al. 2001; Wu et al. 2008; Park et al. 2010). Such interactions between the cross-equatorial SST gradient and antisymmetric wind pattern follow the wind–evaporation–SST (WES) feedback of Xie and Philander (1994), which operates in

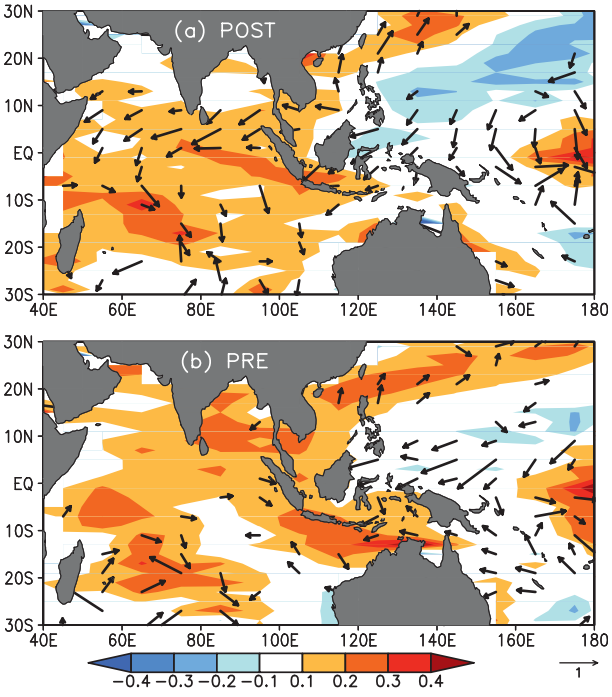


FIG. 11. Regression (color shade) of MAM(1) SST (°C) and wind velocity (m s$^{-1}$) upon NDJ(0) Niño-3.4 SST for (a) the POST (1977–2003) and (b) PRE (1950–76) epochs.

the presence of mean easterlies on either side of the equator. As a result of the WES feedback, NIO SST anomalies are very weak compared to that in the south TIO during the POST epoch. During the PRE epoch, by contrast, MAM(1) SST warming is nearly symmetric across the equator while wind anomalies are weak without a well-defined pattern over the TIO. The antisymmetric wind pattern is not forced by Pacific SST anomalies (see appendix). Du et al. (2009) suggest that it is anchored by the southwest TIO warming associated with the downwelling ocean Rossby waves. Indeed, the warming of the southwest TIO intensifies local atmospheric convection (Xie et al. 2002), exciting cyclonic wind curls during April–June(1) for the POST epoch (Fig. 9). Such a development of cyclonic wind curls does not occur for the PRE epoch, presumably because the Rossby-induced SST warming is weak in the southwest TIO.

Figure 12 compares zonal-mean anomalies of SST and wind in time–latitude sections. The wind and SST anomalies are similar between two epochs until February(1). [The November(0) warming north of the equator is somewhat stronger in the PRE epoch.] From March(1) onward, wind anomalies begin to disintegrate for the PRE epoch while an antisymmetric wind pattern develops and persists through June(1) for the POST epoch. Over the NIO, the anomalous northeasterly winds turn into a warming mechanism after the summer monsoon onset by

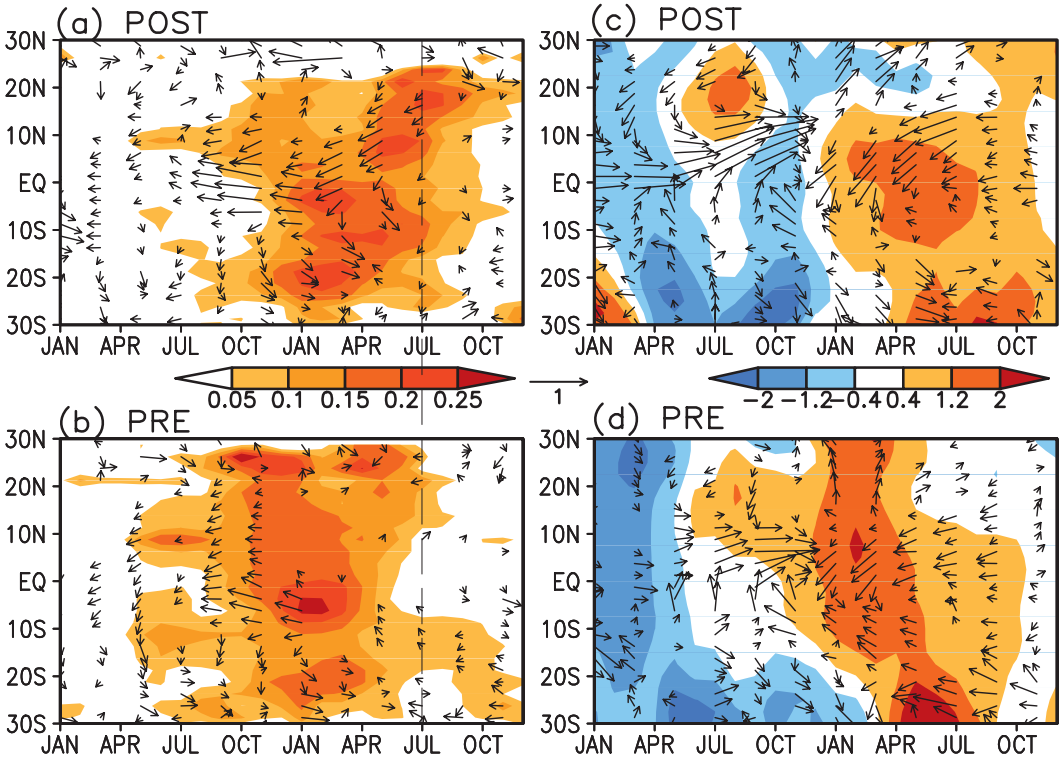


FIG. 12. Regressions upon NDJ(0) Niño-3.4 SST as a function of calendar month and latitude for (a) the POST and (b) PRE epochs: surface wind velocity (m $s^{-1}$) and SST (°C) averaged over TIO (40°–100°E). (c),(d) As in (a),(b) but for ERA tropospheric temperature and iCOADS surface wind averaged over the western Pacific (120°–160°E). POST (PRE) is defined as 1977–2003 (1950–76) for iCOADS, and 1980–2001 (1958–79) for ERA.

weakening the mean southwesterlies and reducing surface turbulent heat flux (Du et al. 2009). As a result of the persistent northeasterly anomalies and shift in the monsoon, the NIO warms for the second time, helping to sustain the TIO warming through JJA(1). The JJA(1) warming over the TIO, especially that over the NIO, anchors the warm Kelvin wave in tropospheric temperature and the anomalous anticyclone in the lower troposphere over the subtropical NW Pacific (Xie et al. 2009; Fig. 12, right panels). Indeed, tropospheric warming over the western Pacific displays a broad equatorial peak from March(1) to August(1) during the POST epoch (Fig. 12c). During the PRE epoch, by contrast, the warming of the tropical troposphere peaks in early year 1, begins to decay in March(1), and is quite weak by July(1) (Fig. 12d).

## 5. East Asian summer rainfall

Interannual variability in summer rainfall over East Asia is complex with a myriad of influential factors; the leading EOF mode typically explains only about 15% of the total variance in the region (Weng et al. 1999; Hsu and Lin 2007). There is a tendency for East Asian rainfall to be correlated with subtropical NW Pacific convection via the PJ pattern (Nitta 1987; Huang and Sun 1992). Recent studies including the present one indicate that TIO SST is an important forcing for the PJ teleconnection. This section examines the relationship between TIO SST and East Asian rainfall in summer and its interdecadal change.

We perform a singular value decomposition (SVD) analysis between East Asian rainfall and TIO SST for 1950–2008, using JJA seasonal mean. Three land precipitation datasets are combined into one single matrix for the analysis to maximize common signals. The use of any one dataset yields qualitatively the same results. The leading mode for rainfall (Fig. 13a) is the so-called tripole pattern, with rainfall increasing in the middle to lower reach of the Yangtze River and decreasing on either side. It represents a sharpening and intensification of the mei-yu rainband over eastern China. This pattern is similar to the leading EOF mode of summer rainfall over East Asia (Weng et al. 1999; Hsu and Lin 2007). The leading mode for SST represents a basinwide warming over the TIO (not shown). The leading mode explains 40% of the covariance and 7% of the rainfall variance.

Figure 13b shows the 21-year running correlation between NDJ(0) ENSO and the rainfall time series of

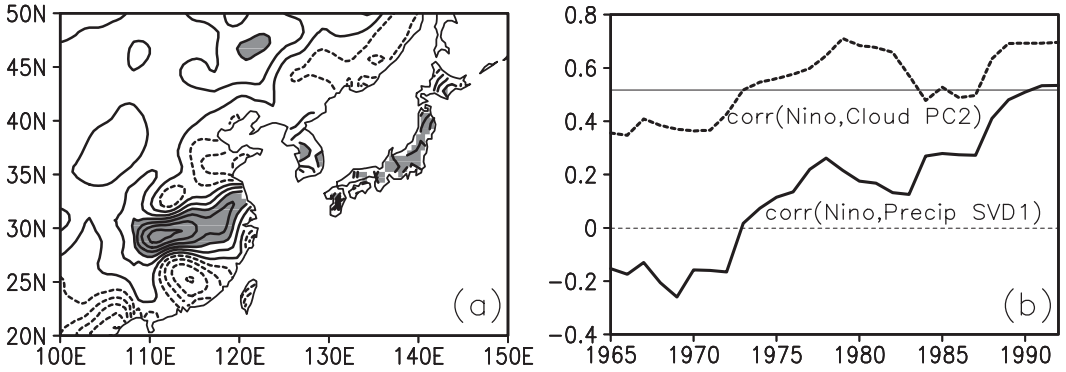


FIG. 13. (a) Rainfall (contours at 5 mm month$^{-1}$ intervals; shaded >10 mm month$^{-1}$) pattern from the SVD analysis with TIO SST for JJA (the time series has been normalized to unit one); (b) 21-year running correlation of the rainfall time series with the NDJ(0) ENSO index.

the leading SVD mode. The correlation is low overall but displays a general rising trend. It rises above the 95% significance level in the late 1980s and stays relatively high since. Superimposed on Fig. 13b is the ENSO correlation with the cloud PC-2 over the eastern Indian and western Pacific Oceans (section 3). The correlation with the JJA(1) cloud mode that features the PJ pattern shows a similar rising trend. It appears that the TIO forcing of the PJ pattern has strengthened, resulting in an increase in ENSO influences on the tripole rainfall pattern over East Asia during JJA(1) since the 1980s.

Convective variability over the subtropical NW Pacific is important to excite the PJ pattern in circulation (Kosaka and Nakamura 2006). Conceivably circulation anomalies of the PJ pattern lead to precipitation changes over East Asia, say by varying the westerly wind jet that is important for the mei-yu–baiu rainband (Sampe and Xie 2010). How circulation affects mei-yu–baiu rainfall and the importance of changes in the mean state are issues that need to be investigated.

## 6. Summary and discussion

Our analysis of ship and land-station observations confirms that the ENSO influence on northwest Pacific climate during the summer JJA(1) strengthened around the mid-1970s, a change documented in Wang et al. (2008) using atmospheric reanalyses. Our results reveal that the TIO warming persists through JJA(1) after, but not before, the climate regime shift. We conclude that during JJA(1), ENSO's influence on the NW Pacific climate and its interdecadal change is indirect and is mediated instead by TIO conditions, given that Pacific SST anomalies are weak and their difference is small between the epochs. Specifically, JJA(1) atmospheric anomalies are robust when TIO SST anomalies are strong, and vice versa. During JJA(1) of the POST epoch, the TIO warming excites a warm Kelvin wave in tropospheric temperature that penetrates into the equatorial Pacific, inducing an anticyclonic circulation and suppressing convection on the northern flank over the subtropical NW Pacific. During the PRE epoch, by contrast, JJA(1) warming over the TIO is weak and so are atmospheric anomalies including the tropospheric Kelvin wave and NW Pacific anticyclone. Coral oxygen isotopic compositions in the central equatorial Indian Ocean show a similar strengthening of correlation with ENSO since the mid-1970s (Timm et al. 2005).

We then proceed to explore what causes the interdecadal change in the TIO warming during JJA(1). Our results confirm the conceptual model of Du et al. (2009) for the TIO warming for the POST epoch. The anticyclonic wind curls during the developing and mature phase of El Niño excite downwelling Rossby waves in the south TIO, inducing SST warming there that persists through June(1). The southwest TIO warming induces an antisymmetric wind pattern that produces a second warming of the NIO by reducing the mean southwesterlies during summer. The NIO warming helps force the warm tropospheric Kelvin wave that affects the circulation and convection over the NW Pacific (Xie et al. 2009). The schematic in Fig. 1 summarizes the mechanisms for the summer NIO warming and its teleconnection.

During the PRE epoch, all of these elements of TIO response to ENSO weaken. ENSO loosens its grip on the TIO as it decays in spring. The south TIO Rossby waves are weaker than in the POST epoch, so are their effect on SST. With the weakened southwest TIO warming, the antisymmetric wind pattern disappears, and the second summer warming fails to develop over the NIO. Losing the anchor in TIO SST, atmospheric anomalies over the NW Pacific during JJA(1) weaken and are not well organized in space.

ENSO strengthened its intensity from the 1960s through 1980s, consistent with its increased influence

on Indo–western Pacific climate after the climate regime shift. The epoch changes in SST and surface wind response over the TIO are asymmetric with respect of the peak of ENSO, larger for the decay than developing phase of ENSO (Figs. 8 and 12). Specifically, the antisymmetric wind pattern and second summer warming of the NIO are very pronounced during the POST but fail to develop during the PRE epoch. To the extent that the antisymmetric wind pattern is due to ocean–atmosphere interaction within the TIO (Wu et al. 2008; Du et al. 2009; Park et al. 2010), its emergence indicates a strengthening of TIO internal feedback during the POST epoch. Indeed, there is evidence that for the past five decades, the thermocline shoals over the southwest TIO thermocline ridge, and the secular SST warming strengthens ocean temperature stratification. Both effects strengthen thermocline feedback, which in turn contributes to an enhanced response of TIO SST to ENSO. Via the capacitor effect, a strong TIO response translates into a pronounced development of atmospheric anomalies over the NW Pacific and East Asia during JJA(1) when ENSO's direct influence fades away.

There is an increasing recognition that each El Niño is different (An and Wang 2000; Trenberth and Smith 2006). Flavors (or features) of individual ENSO events include differences in spatial pattern (between eastern and central Pacific El Niño) and the timing of growth and decay. The pattern and growth flavors can vary ENSO's influence on Indian summer rainfall during year 0 (Kumar et al. 2006; Ihara et al. 2008). Whether an IOD event develops concurrently affects ENSO growth (Annamalai et al. 2005) and termination (Kug et al. 2006). The present study spotlights the decay flavor of ENSO, suggesting that a slow-decaying El Niño induces a more robust response over the TIO and NW Pacific. The interdecadal change in the decay flavor may not be independent of change in ENSO variance. With significant noise present, a weaker ENSO event may appear to decay and lose its coherent structures earlier. In any case, it is important to investigate what determines the decay flavor, an issue important for summer climate prediction for the NW Pacific and East Asia.

Are the epoch changes described here part of ongoing global warming? It is too early to offer a conclusive answer here but some discussions may be warranted given high interest in the topic. First, the secular warming of the TIO since the 1950s is likely among the first signs of global warming (Du and Xie 2008). The warming trend may enhance convective and tropospheric temperature response to interannual anomalies of TIO SST. The enhanced ocean-temperature stratification helps strengthen the TIO basin-warming mode response to El Niño by shoaling the mixed layer and intensifying thermocline feedback in upwelling regions such as the southwest TIO. Second, it is unclear what causes the trend of thermocline shoaling over the southwest TIO and whether it will continue. Global warming projections in many models feature an IOD-like pattern with reduced warming in the eastern and easterly wind anomalies in the central equatorial Indian Ocean (Vecchi and Soden 2007; Du and Xie 2008; Zheng et al. 2010). In these projections, the thermocline deepens in the southwest TIO (Xie et al. 2010), in disagreement with inference from limited observations (Trenary and Han 2008). Finally, while global warming may strengthen ENSO variability (Timmermann et al. 1999), it nevertheless seems too early to tell whether the recent increase in ENSO activity is due to global warming (Wittenberg 2009).

*Acknowledgments.* We wish to thank J. Hafner for obtaining station observations at Guam and Singapore. This work is supported by the U.S. National Science Foundation; the National Aeronautic and Space Administration; the Japan Agency for Marine-Earth Science and Technology; the Chinese Ministry of Education through its support of the Changjiang Scholar and 111 (B07036) Programs, and an overseas fellowship to XTZ; the Qianren Project; the Knowledge Innovation Project of the Chinese Academy of Sciences (KZCX2-YW-BR-04 and KZCX2-YW-220); and the Natural Science Foundation of China (40876007, 40775051, U0733002, and 40830106).

## APPENDIX

### Atmospheric Response to Pacific SST forcing

During MAM(1), El Niño begins to decay while the TIO warming is well developed. Here we use ECHAM5 to study the teleconnection of Pacific SST anomalies during MAM(1). First we construct a composite of SST anomalies for MAM(1) based on observations after 1979, impose as the boundary condition this seasonal-mean map of SST anomalies over the tropical Pacific (20°S–20°N) only (Fig. A1), and integrate the model from 1 February for four months. The same integration is repeated 20 times, with different atmospheric initial conditions each time. We then construct the 20-member ensemble mean difference for MAM(1) from a 20-year simulation with climatological SST.

Figure A1 shows the model surface wind response to Pacific SST forcing. The model reproduces surface wind observations (Fig. 12a) quite well, including westerlies in the equatorial Pacific and an anticyclonic circulation over the NW Pacific. The model results differ markedly

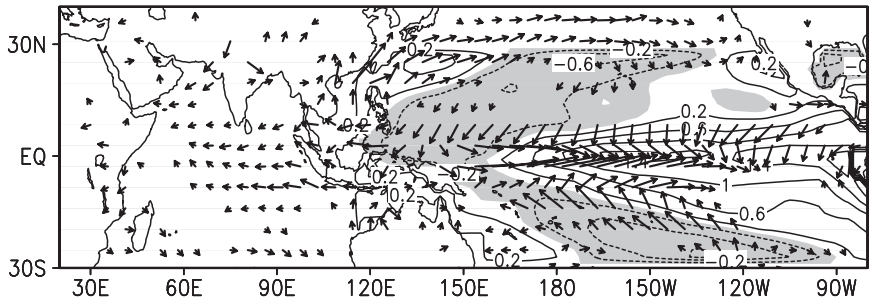


FIG. A1. Twenty-member ensemble-mean ECHAM5 response of surface wind velocity (m $s^{-1}$) to SST anomalies over the tropical Pacific (contour at 0.4°C intervals; negative shaded).

from observations over the TIO. Instead of an antisymmetric pattern, Pacific SST forcing induces easterly wind anomalies in the equatorial Indian Ocean with Ekman downwelling to the south. This result suggests that the antisymmetric wind pattern during MAM(1) over the TIO results from SST anomalies within the basin, a notion corroborated by idealized ECHAM5 experiments of Du et al. (2009, their Fig. 12).

## REFERENCES


Alexander, M. A., I. Blade, M. Newman, J. R. Lanzante, N.-C. Lau, and J. D. Scott, 2002: The atmospheric bridge: The influence of ENSO teleconnections on air–sea interaction over the global oceans. *J. Climate,* **15,** 2205–2231.

Alory, G., S. Wijffels, and G. Meyers, 2007: Observed temperature trends in the Indian Ocean over 1960– 1999 and associated mechanisms. *Geophys. Res. Lett.,* **34,** L02606, doi:10.1029/2006GL028044.

An, S.-I., 2009: A review of interdecadal changes in the nonlinearity of the El Nino-Southern Oscillation. *Theor. Appl. Climatol.,* **97,** 29–40.

——, and B. Wang, 2000: Interdecadal changes in the structure of ENSO mode and their relation to changes of ENSO frequency. *J. Climate,* **13,** 2044–2055.

Annamalai, H., S.-P. Xie, J.-P. McCreary, and R. Murtugudde, 2005: Impact of Indian Ocean sea surface temperature on developing El Niño. *J. Climate,* **18,** 302–319.

Arai, M., and M. Kimoto, 2008: Simulated interannual variation in summertime atmospheric circulation associated with the East Asian monsoon. *Climate Dyn.,* **31,** 435–447.

Ashok, K., S. K. Behera, S. A. Rao, H. Weng, and T. Yamagata, 2007: El Niño Modoki and its possible teleconnection. *J. Geophys. Res.,* **112,** C11007, doi:10.1029/2006JC003798.

Carton, J. A., and B. S. Giese, 2008: A reanalysis of ocean climate using Simple Ocean Data Assimilation (SODA). *Mon. Wea. Rev.,* **136,** 2999–3017.

Chang, C. P., Y. Zhang, and T. Li, 2000: Interannual and interdecadal variations of the East Asian summer monsoon and tropical Pacific SSTs. Part I: Roles of the subtropical ridge. *J. Climate,* **13,** 4310–4325.

Chen, M., P. Xie, J. E. Janowiak, and P. A. Arkin, 2002: Global land precipitation: A 50-yr monthly analysis based on gauge observations. *J. Hydrometeor.,* **3,** 249–266.

Chowdary, J. S., S.-P. Xie, J.-J. Luo, J. Hafner, S. Behera, Y. Masumoto, and T. Yamagata, 2010: Predictability of Northwest Pacific climate during summer and the role of the tropical Indian Ocean. *Climate Dyn.,* doi:10.1007/s00382-009-0686-5.

Collins, W. D., and Coauthors, 2004: Description of the NCAR Community Atmosphere Model (CAM 3.0). Tech. Rep. NCAR/TN-464+STR, National Center for Atmospheric Research, 210 pp.

Deser, C., and M. L. Blackmon, 1995: On the relationship between tropical and North Pacific sea surface temperature variations. *J. Climate,* **8,** 1677–1680.

——, A. S. Phillips, and J. W. Hurrell, 2004: Pacific interdecadal climate variability: Linkages between the Tropics and the North Pacific during boreal winter since 1900. *J. Climate,* **17,** 3109–3124.

Du, Y., and S.-P. Xie, 2008: Role of atmospheric adjustments in the tropical Indian Ocean warming during the 20th century in climate models. *Geophys. Res. Lett.,* **35,** L08712, doi:10.1029/2008GL033631.

——, ——, G. Huang, and K. Hu, 2009: Role of air–sea interaction in the long persistence of El Niño–induced North Indian Ocean warming. *J. Climate,* **22,** 2023–2038.

Garreaud, R. D., and D. S. Battisti, 1999: Interannual and interdecadal variability of the tropospheric circulation in the Southern Hemisphere. *J. Climate,* **12,** 2113–2123.

Gill, A. E., 1980: Some simple solutions for heat-induced tropical circulation. *Quart. J. Roy. Meteor. Soc.,* **106,** 447–462.

Harrison, D., and N. K. Larkin, 1996: The COADS sea level pressure signal: A near-global El Niño composite and time series view, 1946–1993. *J. Climate,* **9,** 3025–3055.

Hsu, H.-H., and S. M. Lin, 2007: Asymmetry of the tripole rainfall pattern during the East Asian summer. *J. Climate,* **20,** 4443–4458.

Huang, B., and J. L. Kinter III, 2002: Interannual variability in the tropical Indian Ocean. *J. Geophys. Res.,* **107,** 3199, doi:10.1029/2001JC001278.

Huang, R.-H., and Y. Wu, 1989: The influence of ENSO on the summer climate change in China and its mechanism. *Adv. Atmos. Sci.,* **6,** 21–32.

——, and F. Sun, 1992: Impacts of the tropical western Pacific on the East Asian summer monsoon. *J. Meteor. Soc. Japan,* **70,** 243–256.

——, W. Chen, B. Yang, and R. Zhang, 2004: Recent advances in studies of the interaction between the East Asian winter and summer monsoons and ENSO cycle. *Adv. Atmos. Sci.,* **21,** 407–424.

Ihara, C., Y. Kushnir, M. A. Cane, and A. Kaplan, 2008: Timing of El Niño–related warming and Indian summer monsoon rainfall. *J. Climate,* **21,** 2711–2719.

Izumo, T., C. B. Montégut, J.-J. Luo, S. K. Behera, S. Masson, and T. Yamagata, 2008: The role of the western Arabian Sea upwelling in Indian monsoon rainfall variability. *J. Climate,* **21,** 5603–5623.

Kalnay, E., and Coauthors, 1996: The NCEP/NCAR 40-Year Reanalysis Project. *Bull. Amer. Meteor. Soc.,* **77,** 437–471.

Kawamura, R., T. Matsumura, and S. Iizuka, 2001: Role of equatorially asymmetric sea surface temperature anomalies in the Indian Ocean in the Asian summer monsoon and El Nino–Southern Oscillation coupling. *J. Geophys. Res.,* **106D,** 4681–4693.

Klein, S. A., B. J. Soden, and N.-C. Lau, 1999: Remote sea surface temperature variations during ENSO: Evidence for a tropical atmospheric bridge. *J. Climate,* **12,** 917–932.

Kosaka, Y., and H. Nakamura, 2006: Structure and dynamics of the summertime Pacific–Japan teleconnection pattern. *Quart. J. Roy. Meteor. Soc.,* **132,** 2009–2030.

Kubota, T., and T. Terao, 2004: Interdecadal variability of the seasonal-scale persistence in the tropical mean tropospheric temperature. *J. Meteor. Soc. Japan,* **82,** 1213–1221.

Kucharski, F., A. Bracco, J. H. Yoo, A. Tompkins, L. Feudale, P. Ruti, and A. dell'Aquila, 2009: A Gill-Matsuno-type mechanism explains the tropical Atlantic influence on African and Indian monsoon rainfall. *Quart. J. Roy. Meteor. Soc.,* **135,** 569–579.

Kug, J.-S., T. Li, S.-I. An, I.-S. Kang, J.-J. Luo, S. Masson, and T. Yamagata, 2006: Role of the ENSO–Indian Ocean coupling on ENSO variability in a coupled GCM. *Geophys. Res. Lett.,* **33,** L09710, doi:10.1029/2005GL024916.

Kumar, K. K., B. Rajagopalan, M. Hoerling, G. Bates, and M. Cane, 2006: Unraveling the mystery of Indian Monsoon failure during El Niño. *Science,* **314,** 115–119.

Legates, D. R., and C. J. Willmott, 1990: Mean seasonal and spatial variability in gauge-corrected, global precipitation. *Int. J. Climatol.,* **10,** 111–127.

Lau, N.-C., and M. J. Nath, 2003: Atmosphere–ocean variations in the Indo-Pacific sector during ENSO episodes. *J. Climate,* **16,** 3–20.

Mantua, N. J., S. R. Hare, Y. Zhang, J. M. Wallace, and R. C. Francis, 1997: A Pacific interdecadal climate oscillation with impacts on salmon production. *Bull. Amer. Meteor. Soc.,* **78,** 1069–1079.

Matsuno, T., 1966: Quasi-geostrophic motions in the equatorial area. *J. Meteor. Soc. Japan,* **44,** 25–43.

Minobe, S., 1997: A 50–70 year climatic oscillation over the North Pacific and North America. *Geophys. Res. Lett.,* **24,** 683–686.

Nitta, T., 1987: Convective activities in the tropical western Pacific and their impact on the Northern Hemisphere summer circulation. *J. Meteor. Soc. Japan,* **65,** 373–390.

——, 1990: Unusual summer weather over Japan in 1988 and its relationship to the Tropics. *J. Meteor. Soc. Japan,* **68,** 575–588.

——, and S. Yamada, 1989: Recent warming of tropical sea surface temperature and its relationship to the Northern Hemisphere circulation. *J. Meteor. Soc. Japan,* **67,** 375–383.

Ohba, M., and H. Ueda, 2006: A role of zonal gradient of SST between the Indian Ocean and the western Pacific in localized convection around the Philippines. *Sci. Onl. Lett. Atmos.,* **2,** 176–179.

Park, H.-S., J. C. H. Chiang, B. R. Lintner, and G. J. Zhang, 2010: The delayed effect of major El Niño events on Indian monsoon rainfall. *J. Climate,* **23,** 932–946.

Power, S., T. Casey, C. Folland, A. Colman, and V. Mehta, 1999: Inter-decadal modulation of the impact of ENSO on Australia. *Climate Dyn.,* **15,** 319–324.

Rao, S. A., and S. K. Behera, 2005: Subsurface influence on SST in the tropical Indian Ocean: Structure and interannual variability. *Dyn. Atmos. Oceans,* **39,** 103–135.

Roeckner, E., and Coauthors, 2003: Atmospheric General Circulation Model ECHAM5: Part I. Tech. Rep. 349, Max-Planck-Institut für Meteorlogie, 140 pp.

Rudolf, B., and U. Schneider, 2005: Calculation of gridded precipitation data for the global land-surface using in-situ gauge observations. *Proc. Second Workshop of the Int. Precipitation Working Group IPWG,* Monterey, CA, CGMS, 231-247.

Saji, N. H., B. N. Goswami, P. N. Vinayachandran, and T. Yamagata, 1999: A dipole mode in the tropical Indian Ocean. *Nature,* **401,** 360–363.

Sampe, T., and S.-P. Xie, 2010: Large-scale dynamics of the meiyu–baiu rainband: Environmental forcing by the westerly jet. *J. Climate,* **23,** 113–134.

Sasaki, H., M. Nonaka, Y. Masumoto, Y. Sasai, H. Uehara, and H. Sakuma, 2008: An eddy-resolving hindcast simulation of the quasi-global ocean from 1950 to 2003 on the Earth Simulator. *High Resolution Numerical Modelling of the Atmosphere and Ocean,* W. Ohfuchi and K. Hamilton, Eds., Springer, 157–186.

Schott, F. A., S.-P. Xie, and J. P. McCreary, 2009: Indian Ocean circulation and climate variability. *Rev. Geophys.,* **47,** RG1002, doi:10.1029/2007RG000245.

Taguchi, B., S.-P. Xie, N. Schneider, M. Nonaka, H. Sasaki, and Y. Sasai, 2007: Decadal variability of the Kuroshio Extension: Observations and an eddy-resolving model hindcast. *J. Climate,* **20,** 2357–2377.

Terao, T., and T. Kubota, 2005: East-west SST contrast over the tropical oceans and the post El Niño western North Pacific summer monsoon. *Geophys. Res. Lett.,* **32,** L15706, doi:10.1029/2005GL023010.

Timm, O., M. Pfeiffer, and W.-C. Dullo, 2005: Nonstationary ENSO-precipitation teleconnection over the equatorial Indian Ocean documented in a coral from the Chagos Archipelago, *Geophys. Res. Lett.,* **32,** L02701, doi:10.1029/2004GL021738.

Timmermann, A., J. Oberhuber, A. Bacher, M. Esch, M. Latif, and E. Roeckner, 1999: Increased El Nino frequency in a climate model forced by future greenhouse warming. *Nature,* **398,** 694–697.

Trenary, L. L., and W. Han, 2008: Causes of decadal subsurface cooling in the tropical Indian Ocean during 1961–2000. *Geophys. Res. Lett.,* **35,** L17602, doi:10.1029/2008GL034687.

Trenberth, K. E., and J. W. Hurrell, 1994: Decadal atmospheric-ocean variations in the Pacific. *Climate Dyn.,* **9,** 303–319.

——, and L. Smith, 2006: The vertical structure of temperature in the Tropics: Different flavors of El Niño. *J. Climate,* **19,** 4956–4973.

Uppala, S. M., and Coauthors, 2005: The ERA-40 reanalysis. *Quart. J. Roy. Meteor. Soc.,* **131,** 2961–3012.

Vecchi, G. A., and B. J. Soden, 2007: Global warming and the weakening of the tropical circulation. *J. Climate,* **20,** 4316–4340.

Wang, B., R. Wu, and T. Li, 2003: Atmosphere–warm ocean interaction and its impact on Asian–Australian monsoon variability. *J. Climate,* **16,** 1195–1211.

——, Q. Ding, X. Fu, I.-S. Kang, K. Jin, J. Shukla, and F. Doblas-Reyes, 2005: Fundamental challenge in simulation and prediction of summer monsoon rainfall. *Geophys. Res. Lett.,* **32,** L15711, doi:10.1029/2005GL022734.

——, J. Yang, T. Zhou, and B. Wang, 2008: Interdecadal changes in the major modes of Asian–Australian monsoon variability: Strengthening relationship with ENSO since the late 1970s. *J. Climate,* **21,** 1771–1789.

Wang, C., R. H. Weisberg, and J. I. Virmani, 1999: Western Pacific interannual variability associated with the El Niño–Southern Oscillation. *J. Geophys. Res.,* **104D,** 5131–5149.

Webster, P. J., A. M. Moore, J. P. Loschnigg, and R. R. Leben, 1999: Coupled oceanic-atmospheric dynamics in the Indian Ocean during 1997-98. *Nature,* **401,** 356–360.

Weng, H.-Y., K.-M. Lau, and Y.-K. Xue, 1999: Multi-scale summer rainfall variability over China and its long-term link to global sea surface temperature variability. *J. Meteor. Soc. Japan,* **77,** 845–857.

White, W. B., 1995: Design of a global observing system for gyre-scale upper ocean temperature variability. *Progr. Oceanogr.,* **36,** 169–217.

Wittenberg, A. T., 2009: Are historical records sufficient to constrain ENSO simulations? *Geophys. Res. Lett.,* **36,** L12702, doi:10.1029/2009GL038710.

Worley, S. J., S. D. Woodruff, R. W. Reynolds, S. J. Lubker, and N. Lott, 2005: ICOADS release 2.1 data and products. *Int. J. Climatol.,* **25,** 823–842.

Wu, G. X., and H. Liu, 1995: Neighborhood response of rainfall to tropical sea surface temperature anomalies. Part I: Numerical experiment. *Chin. J. Atmos. Sci.,* **19,** 422–434.

Wu, R., and B. Wang, 2002: A contrast of the East Asian summer monsoon–ENSO relationship between 1962–77 and 1978–93. *J. Climate,* **15,** 3266–3279.

——, and S.-P. Xie, 2003: On equatorial Pacific surface wind changes around 1977: NCEP–NCAR reanalysis versus COADS observation. *J. Climate,* **16,** 167–173.

——, B. P. Kirtman, and V. Krishnamurthy, 2008: An asymmetric mode of tropical Indian Ocean rainfall variability in boreal spring. *J. Geophys. Res.,* **113,** D05104, doi:10.1029/2007JD009316.

Xie, S.-P., and S. G. H. Philander, 1994: A coupled ocean-atmosphere model of relevance to the ITCZ in the eastern Pacific. *Tellus,* **46A,** 340–350.

——, H. Annamalai, F. A. Schott, and J. P. McCreary, 2002: Structure and mechanisms of South Indian Ocean climate variability. *J. Climate,* **15,** 864–878.

——, Q. Xie, D. X. Wang, and W. T. Liu, 2003: Summer upwelling in the South China Sea and its role in regional climate variations. *J. Geophys. Res.,* **108,** 3261, doi:10.1029/2003JC001867.

——, K. Hu, J. Hafner, H. Tokinaga, Y. Du, G. Huang, and T. Sampe, 2009: Indian Ocean capacitor effect on Indo–western Pacific climate during the summer following El Niño. *J. Climate,* **22,** 730–747.

——, C. Deser, G. A. Vecchi, J. Ma, H. Teng, and A. T. Wittenberg, 2010: Global warming pattern formation: Sea surface temperature and rainfall. *J. Climate,* **23,** 966–986.

Yang, J., Q. Liu, S.-P. Xie, Z. Liu, and L. Wu, 2007: Impact of the Indian Ocean SST basin mode on the Asian summer monsoon. *Geophys. Res. Lett.,* **34,** L02708, doi:10.1029/2006GL028571.

Yu, W., B. Xiang, L. Liu, and N. Liu, 2005: Understanding the origins of interannual thermocline variations in the tropical Indian Ocean. *Geophys. Res. Lett.,* **32,** L24706, doi:10.1029/2005GL024327.

Zhang, R. H., A. Sumi, and M. Kimoto, 1996: Impact of El Nino on the East Asian monsoon: A diagnostic study of the 1986/87 and 91/92 events. *J. Meteor. Soc. Japan,* **74,** 49–62.

Zhang, Y., J. M. Wallace, and D. S. Battisti, 1997: ENSO-like interdecadal variability: 1900-93. *J. Climate,* **10,** 1004–1020.

Zheng, X.-T., S.-P. Xie, G. A. Vecchi, Q. Liu, and J. Hafner, 2010: Indian Ocean dipole response to global warming: Analysis of ocean–atmospheric feedbacks in a coupled model. *J. Climate,* **23,** 1240–1253.

Zhou, T., D. Gong, J. Li, and B. Li, 2009: Detecting and understanding the multi-decadal variability of the East Asian summer monsoon—Recent progress and state of affairs. *Meteor. Z.,* **18,** 455–467.